International Journal of Applied Earth Observations and Geoinformation 98 (2021) 102315

Contents lists available at ScienceDirect

International Journal of Applied Earth Observations and Geoinformation

journal homepage: www.elsevier.com/locate/jag

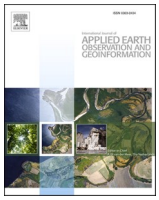

Quantifying river ice movement through a combination of European satellite monitoring services

Bas Altena [a,b,*], Andreas Kääb [a]

[a] Department of Geosciences, University of Oslo, Norway
[b] Institute for Marine and Atmospheric research, Utrecht University, the Netherlands

ARTICLE INFO

Keywords:
Sentinel-2
PROBA-V
River-ice movement monitoring
Multi-sensor
Mini-satellite

2010 MSC:
00-01
99-00

ABSTRACT

Every spring the mechanical river ice break-up and associated ice-runs or flooding pose a threat to communities at Northern latitudes. Monitoring and mitigation efforts along remote Arctic rivers are possible but logistically complex. In recent years, Earth observation programs have emerged based on spaceborne sensors that record large parts of the Earth's surface at a regular interval and with fast downlink. Most optical satellites have a similar sun-synchronous orbit, and have thus an akin ground track. When different sun-synchronous missions are combined this results in near-simultaneous acquisitions, which make it possible to monitor fast displacements that occur at or near the Earth's surface over large scales. Hence, it becomes possible to generate a new monitoring system; one of observing river ice movement. In this study we demonstrate the feasibility of a multi-satellite monitoring system by combining data from freely available medium- and coarse-resolution satellites, in this study that is Sentinel-2 and PROBA-V. Velocities of floating river ice during the spring of 2016 are estimated over a more than 700 km long reach of the Lena River in Russia. In order to achieve automatic velocity estimates at such scales, efficient and river-ice specific processing steps are included. Entropy filters are used to detect regions of high contrast and neglects open water or an intact ice cover, and also help the image matching. Post-processing is done through filtering on the general flow direction, stemming from a global river mask dataset. In all, this study shows the potential of extracting river ice movement from a combination of low and medium resolution satellite sensors in sun-synchronous orbit.

1. Introduction

Remote sensing of surface water is mostly concerned with mapping the extent of water bodies (Huang et al., 2018). For seasonally frozen rivers, remote sensing also enables (or involves) ice cover classification and determining the timing of break-up (Chaouch et al., 2014; Cooley and Pavelsky, 2016), its progression through time series (Zhang et al., 2017) or localizing its potential initiation regions (Lindenschmidt and Das, 2015). One little exploited aspect is the possibility to extract ice displacement data from near-simultaneous optical remote sensing data. Given this approach, water surface velocities can be extracted and these resultis can be used to supplement discharge estimation from space, which currently relies on scaling laws (Gleason and Smith, 2013).

The possibilities for the estimation of large-scale river ice displacement from space has been demonstrated (Kääb and Prowse, 2011; Kääb et al., 2013; Beltaos and Kääb, 2014; Kääb et al., 2019). In this study we expand upon this principle and highlight the possibilities of combining data from different satellite systems. We explore also the potential of extracting such river ice displacements from coarse resolution satellite images. While the work of Kääb et al. (2013) was based upon data from essentially tasked acquisitions of the Terra ASTER instrument, the data in this study is freely available and acquired throughout most of the sun-lit part of both satellite orbits ("always on" mode).

Apart from cubesats (Kääb et al., 2019), currently no other satellite (constellation) has capabilities for systematic river ice movement extraction. An optical system for river ice movement would need either a companion satellite, or stereoscopic telescopes. Very few such systems are currently in space, hence an ad-hoc strategy of combining different satellites, as presented here, is the most feasible option. Imaging microwave sensors might be another alternative, but there lacks a clear demonstration of observing movement of river ice debris (or floes). However, displacements based upon spaceborne SAR data have been demonstrated through inSAR over frozen lakes and estuaries (Vincent et al., 2004), or speckle tracking over landfast sea ice (Choe et al., 2020).

* Corresponding author at: Department of Geosciences, University of Oslo, Norway.
E-mail addresses: bas.altena@geo.uio.no (B. Altena), kaeaeb@geo.uio.no (A. Kääb).

https://doi.org/10.1016/j.jag.2021.102315
Received 31 March 2020; Received in revised form 29 January 2021; Accepted 4 February 2021
Available online 27 February 2021

Table 1
Sensor characteristics of the MSI instrument on Sentinel-2, and of the central, nadir-looking instrument on PROBA-V satellite.

satellite	Sentinel-2				PROBA-V				units
field of view	20.6				34				deg
swath width	290				500				km
compression	JPEG2000				CCSDS				
bands	blue	green	red	NIR	blue	red	NIR	SWIR	
spatial resolution	10	10	10	10	100	100	100	200	m
central wavelength	0.490	0.560	0.665	0.842	0.463	0.655	0.845	1.600	μm
signal-to-noise	154	168	142	174	115	430	529	380	[·]

These just mentioned case studies use data with a time separation in the order of days, hence such methods can be used for measuring slow changes of the ice cover such as horizontal deformation or tiny vertical displacements, but not for fast occurring break-up events and associated ice transport. Shorter intervals are possible through decomposition of an individual SAR image, but have only been demonstrated on sea ice (Kræmer et al., 2017). In addition, these techniques extract line-of-sight displacement, thus only one component of the three dimensional velocity vector is resolved. Similar to optical remote sensing, the most straight forward implementation for such a system would thus be to use companion satellites. TanDEM-X is such a configuration, but this system has already surpassed its satellite lifetime and the temporal separation of the two was normally too short. In the future, the ESA Earth Explorer 10 candidate mission of Harmony, which are two companion satellites flying alongside the Sentinel-1D satellite, might be a system able to generate such products, through along-track interferometry. However, this mission is currently in its feasibility phase. While not ideal, the use of different sun-synchronous optical satellite seems to be a feasible strategy to construct a river ice monitoring system, given all options above.

River ice velocities can be of help to transfer discharge retrievals to gauging stations (Kääb et al., 2019), complementing more common river width and altimetric methodologies (Smith and Pavelsky, 2008) from space. Apart from hydrological modeling the configuration used in this study can be of interest for environmental risk mitigation. It has the potential for developing a monitoring system with already existing spaceborne Earth observation missions. Its value is mostly found in the possibility to generate a product in near real-time, as the fast availability of the imagery creates low latency, and the processing is technically a simple implementation. This data cadence is a prerequisite for flood warnings (Allen et al., 2018), or in the case of ice jam break-up, the violent flood peaks. Such ice jam releases, called javes, propagate faster than the ice rubble itself at velocities of 5 $m \cdot s^{-1}$ (Beltaos and Burrell, 2005; Kowalczyk Hutchison and Hicks, 2007).

From an engineering perspective, the mapping of the flow structure is of interest as ice jams are of limited spatial extent and short-lived events. Given the vast stretches of Arctic rivers, it is evident to use spaceborne remote sensing as a mapping tool. Alternatively, river velocities extraction from images acquired from aerial (Dugan et al., 2013) or drone (Lewis and Rhoads, 2018) platforms is possible, but only for small river regions or reaches. In this study, we demonstrate the feasibility of a large scale monitoring system by combining data from the medium resolution satellite Sentinel-2 and the coarse resolution satellite PROBA-V.

The structure of this study is as follows; the next section describes the configuration and sensor specifics of both optical satellite systems. This is followed by a brief section about the study area. Then the methodology of the different steps within the processing pipeline is presented. Hereafter, the results of our implementation are tested over several hundred kilometers of the Lena River. Results are shown within a week of break-up, where for two different days there are clear sky or hazy conditions. The paper concludes with a discussion on the potential of this method for current satellite systems and its potential for companion mini-satellites in the future.

2. Near-simultaneous satellite constellations

2.1. Instrument description of Sentinel-2

Sentinel-2 is a tandem mission, where two satellites fly in concert along a similar orbital plane, resulting in a revisit of the same orbital track every five days. The optical instrument on board both satellites is a multi-spectral linescanner (MSI) sensitive to light from the visible up to the shortwave infrared spectrum, see also Table 1. The spatial resolution of the scanner varies from 10 up to 60 m, depending on spectral bands, and its swath-width is ≈270 km. These sensors are an integrated part of the Copernicus monitoring program, and thus acquire almost continuously throughout their sun-lit orbit (Drusch et al., 2012; Gascon et al., 2017). In its current configuration all parts of the Earth's surface are sensed every five days by the Sentinel-2 constellation,[1] with even shorter sensing rates at high latitude due to orbital convergence towards the poles (Kääb et al., 2016).

2.2. Instrument description of PROBA-V

The PROBA-V mini-satellite has a single focused objective, as it tries to continue the SPOT-vegetation legacy (Francois et al., 2014). This SPOT mission had been in place since 1998. However, the SPOT5 vegetation satellite is now decommissioned from its main objective and the PROBA-V satellite fills the gap between the time-series from the SPOT family and the tandem satellites of the Sentinel-3 mission (Donlon et al., 2012). On board of the PROBA-V satellite are three telescopes, with line scanners sensitive to light in the visible and shortwave spectrum. From these three telescopes, the nadir-looking pushbroom instrument has a swath-width of 500 km. Four spectral bands are recorded, with three in the (far-)visible range and at a spatial resolution of 100 m, and one in the shortwave infrared (SWIR) at 200 m, see Table 1. The nadir recording telescope is complemented by two side-looking telescopes, with similar spectral specifications but a lower spatial resolution up to 300 m on the ground. The combined swath-width of all three instruments is ≈2285 km. However in this study, we only use data from the nadir-looking telescope.

2.3. High-latitude acquisitions of PROBA-V

The initial mission objective of PROBA-V was to monitor land cover (Dierckx et al., 2014), thus its recording strategy has been focused on mid-latitudes. Though there is potential for PROBA-V to be of use for Arctic research and monitoring, as will be shown in this contribution. Unfortunately, PROBA-V used a cut-off angle for low sun illumination at 8°, which is higher than for Sentinel-2 and Landsat. This means that when the sun is at its lowest point in December during winter solstice, all potential imagery above 57.5° North are not recorded (Hawotte et al., 2016). For river ice monitoring this will affect availability of imagery during the freeze-up period (in late autumn and early winter), but solar

[1] https://sentinel.esa.int/web/sentinel/missions/sentinel-2/acquisition-plans.

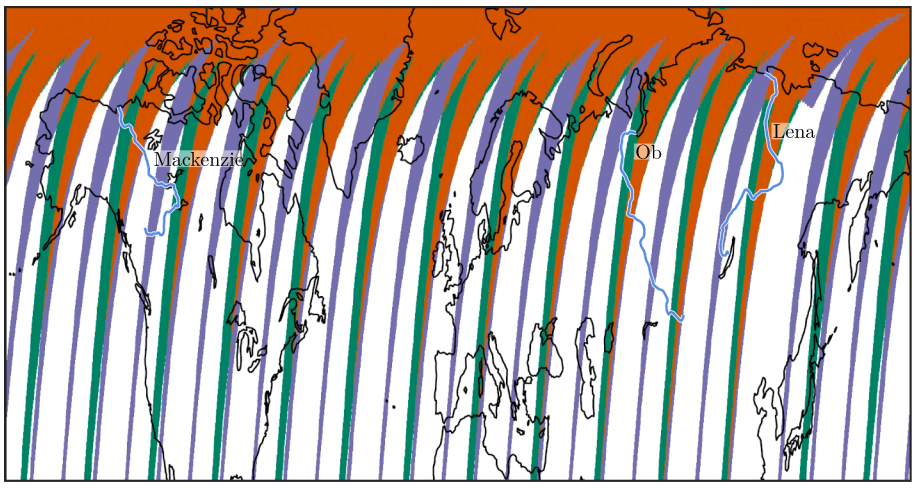

Fig. 1. Ground coverage acquired during one day in the Northern hemisphere, for Sentinel-2A & 2B (purple), PROBA-V's nadir instrument (green) and where the swaths of both sensors overlap (orange). In addition, three great Arctic rivers are highlighted in blue. (For interpretation of the references to color in this figure legend, the reader is referred to the web version of this article.)

Table 2
Envisioned characteristics of the satellite systems.

	Sentinel-2	PROBA-V	units
inclination	98.62	98.8	deg
altitude	786	820	km
local crossing time at equator	10:30	10:20	hh:mm

elevation will be sufficiently high when break-up occurs in spring (though break-up events can occur for some rivers and conditions in mid-winter (Prowse et al., 2007)). Sometimes PROBA-V acquired imagery over the polar regions. For example, in 2015–2016 the satellite had a season where it acquired at lower sun illumination angles, and in 2018–2019 it had an imaging campaign over Antarctica. Because such experimental programs are now implemented, it becomes possible to demonstrate this concept also for high-latitude river ice monitoring.

2.4. Orbital inclination angle

Both PROBA-V and the Sentinel-2 satellites are set in sun-synchronous orbit at inclinations of 98.5° and 98.6°, respectively. This orbit type is popular in Earth observation, as in this way the sun azimuth is relatively stable throughout the year, thus changes in illumination and associated shadows vary little between the acquisitions, which is of ease for (automatic) photo-interpretation. Because the satellite orbits are of such similar orientation, the paths of both satellite systems are very similar. Hence the spatial overlap of both satellites covers a large area, it is not just some occasional crossing (Fig. 1).

2.5. Equatorial crossing time

Along with the spatial similarity of the orbit, both satellites also have a similar overpass time (see Table 2). Most sun-synchronous systems cross the equator close to local noon. This makes it possible to have near simultaneous over-passes for combinations of local noon satellite systems, which is needed for river-ice monitoring (Kääb and Leprince, 2014). However, like any satellite, the gravitational pull of the Earth brings the satellites back down. In order to stay in a stable orbit, most satellites have thrusters, which use fuel carried on board, which is a limiting resource. The envisioned mission life time of PROBA-V was 2.5 years (Francois et al., 2014), and this was even extended with an additional five years. Nevertheless, the fuel for the boosters is limited, and thus orbit maneuvers are kept to the minimum. Consequently, PROBA-V has more drift in its equatorial crossing time, as can be seen in Fig. 2. Hence due to this variability in crossing-time of PROBA-V, the results presented here can unfortunately not be implemented throughout the whole lifespan of this mission, as the time separation needs to be within a certain time window.

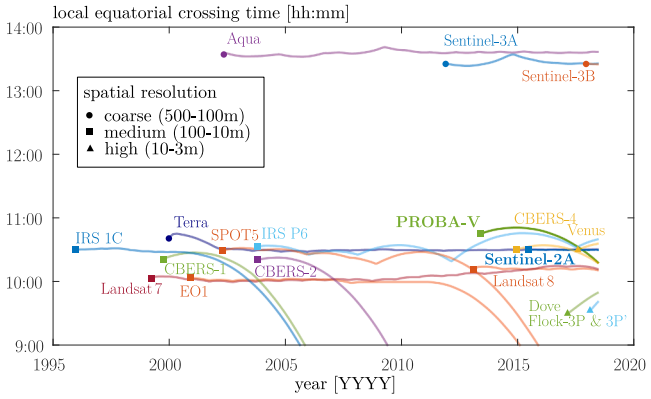

Fig. 2. The local equatorial crossing time as time progresses for a selection of sun-synchronous optical Earth observation platforms.

3. Study site

Lena River is a 4400 km long river in Russia, which has its source at Lake Baikal and ends in a delta, flowing into the Arctic ocean. The basin lies in a zone of continental moderate and sub-arctic climate (Hudson and Thompson, 2019). A large portion of the winter precipitation accumulates as snow and this capacity is released in spring. One factor contributing to increased spring release is the permafrost-rich environment Lena River is situated in, as an impermeable surface layer of frozen soil has created a limited storage capacity.

Discharge of Lena River is in the order of ≈30,000 $m^3\ s^{-1}$ or ≈530 $km^3\ a^{-1}$ at the delta. Its discharge is highly skewed as the spring flood discharge shows typically a twenty-fold increase in relation to the low flow condition in autumn. On decadal scales the average water discharge has increased (Fedorova et al., 2015), as well as monthly discharges in late spring and summer (Ye et al., 2004). At Tabaga at least 600 km upstream of our study region, the peak discharge typically occurs in May and these events typically last for some days (Gautier et al., 2018).

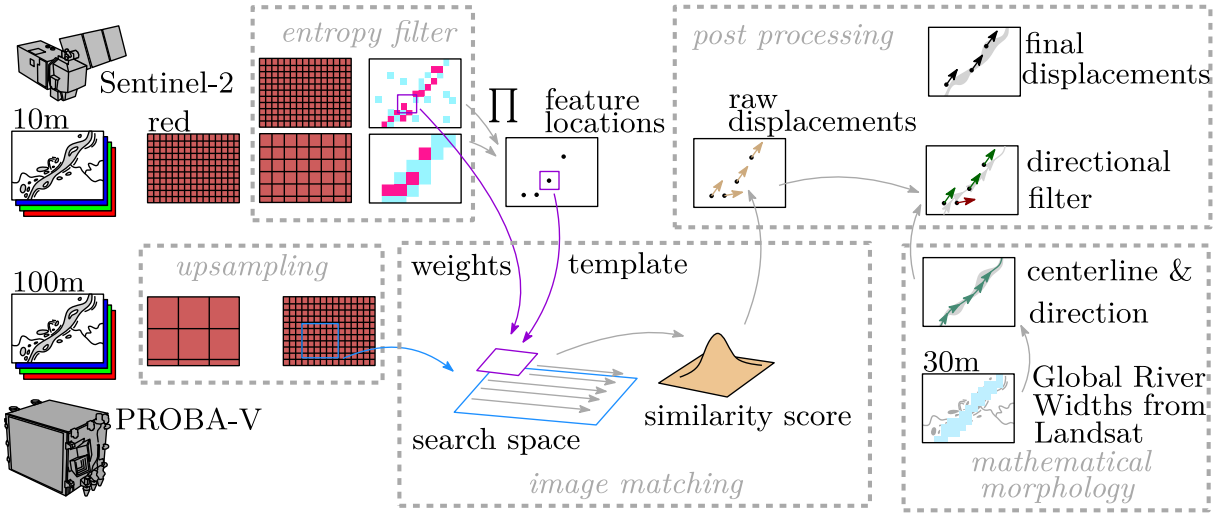

Fig. 3. Schematic of the top level workflow in this study.

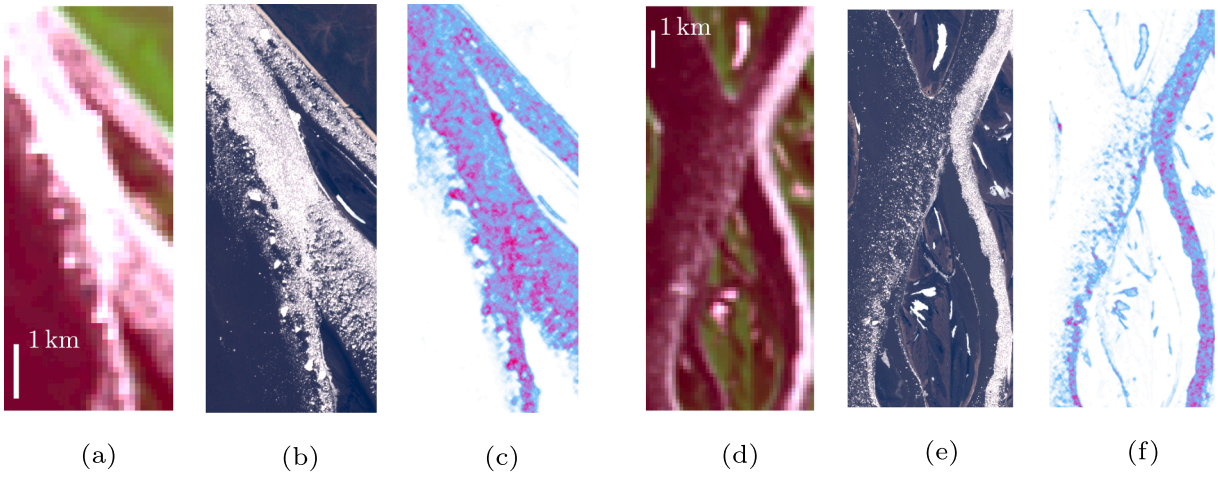

Fig. 4. (a, d) Subsets of PROBA-V and (b, e) Sentinel-2 imagery from spring 2017. The weighting function, based upon multiple entropy filters, is also shown (c, f) for the same sections. Where, white are low values, blue intermediate, and purple denote high entropy. The location of these image subsets are N:67°18′18″ E:123°14′30″ and N:67°02′47″ E:123°29′47″ and close to the village of Kystatyam.

The region under study is an almost 700 km long reach of the lower part of Lena River. In the southern portion of this reach the river is relatively braided where the flood plain can be up to 40 km wide and the river can occupy up to 15 km in width when it spreads into a multiple-channel system. In our study region this system transits into a single channel system with a width of roughly 3 km. While the topography around the river consists in the East of hills up to 500 m in elevation, while the western part is relatively flat with an abundance of permafrost features. This permafrost plain gradually changes into more topographic variation, causing Lena River to run through a canyon, where the gauging station of Kyusyur is situated. Just south of our study extent is the region analyzed by Smith and Pavelsky (2008).

4. Method

The focus of this work is to show the feasibility of a monitoring system for river ice flow from space. Hence, in the following section we will discuss the implementation details of our river ice velocity pipeline (Fig. 3). We try in particular to keep the processing time low. Low latency is important, but is hampered by the procedure of image matching, which is computationally expensive. Thus additional building blocks are included and described. In short we start with the localization of the river and its ice floes, followed by tracking image similarity to extract displacements. Finally, the filtering of outliers from the raw velocity measurements is explained.

4.1. River and ice flow localization

Localization needs to be done on two levels, first the location of the river. Secondly, the ice-floes within the imagery need to be identified for the image matching. General localization of the river is done through a preexisting river mask, which is based on Landsat water classification at 30 m resolution (Allen and Pavelsky, 2018).[2] Localization of ice floes is of importance as usually matching is done on a regular grid in a naive fashion, i.e. the sampling grid is taken independently of the image content. However by doing so, displacements are also estimated along stagnant border ice or ice-free water sections. Moving ice floes might only occupy a small subset of total river width at some places, especially when clearance has occurred. Thus the image dataset is used to detect ice floes and this is used to select positions for the displacement sampling.

[2] available at https://zenodo.org/record/1269595.

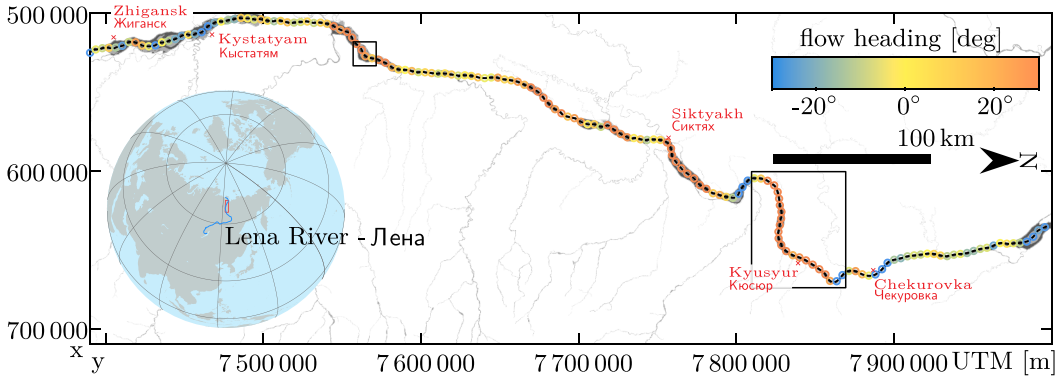

Fig. 5. Estimate of the general heading of flow for Lena river, where the river center line is plotted in gray, while the colors indicate the off-North heading in degrees. The inserted globe outlines the extent of the study region in red. (For interpretation of the references to color in this figure legend, the reader is referred to the web version of this article.)

In order to locate ice floes in the imagery we deploy an entropy filter, which is formulated as (Gonzalez and Woods, 2002),

$$\mathbf{H}_q = -\sum_{k,l} p(\mathbf{I}_q(k,l)) \log p(\mathbf{I}_q(k,l)). \tag{1}$$

Here $p()$ denotes the probability function, which can be calculated by a normalized sample histogram. This histogram is calculated over a subset of an image ($\mathbf{I}_q$). The extent of this neighborhood is given by whole integers k and l. Thus a rectangular subset surrounding a pixel is sampled, in our case the range of k and l spans from $-3\ldots+3$ till $-7\ldots+7$. A clear separation is established between homogeneous snowy banks and open water from patchy unordered ice-floes, when output of entropy at different scales are multiplied. An example of the response from multi-scale entropy filters over a medium resolution Sentinel-2 image are shown in Fig. 4.

The entropy filters are normalized and multiplied ($\prod p(\mathbf{H}_q)$), then a threshold of 0.6 is set on the resulting response. This cut-off enforces a selection on locations that are only present in the upper quantiles at every spatial scale ($0.90^5 = 0.59$). It is at these locations where image matching will be applied. This feature-based strategy is commonly used in orientation problems or topographic reconstruction and considerably reduces the processing time.

4.2. Image correlation and displacement extraction

There is knowledge on the locations of ice floes in one image through entropy filtering, but there is not yet knowledge about the direction and magnitude of the traveling ice rubble. Hence displacement estimation from optical remote sensing uses naive image matching over a regular grid, independent of the image content. The method is based on extracting a small template from one image and finding the most similar pattern in a larger region of another image. The similarity measure (Θ) is implemented through normalized cross-correlation (NCC), and can be formulated as (Brown, 1992),

$$\Theta_{pq} = \frac{\sum_{k,l}(\mathbf{I}_p(i+k,j+l) - \overline{\mathbf{I}}_p)(\mathbf{I}_q(k,l) - \overline{\mathbf{I}}_q)}{\sqrt{\sum_{k,l}(\mathbf{I}_p(i+k,j+l) - \overline{\mathbf{I}}_p)^2 \sum_{k,l}(\mathbf{I}_q(k,l) - \overline{\mathbf{I}}_q)^2}}. \tag{2}$$

Here Θ_{pq} denotes a score surface at discrete step sizes (i,j), that span a search space. The location with the highest correlation score in this search space is taken as the displacement estimate. The individual correlation scores are calculated by the similarity of two smaller templates ($\mathbf{I}_p$ & $\mathbf{I}_q$). In this formulation, the normalized cross-correlation is used in which templates are transformed to variations by their mean intensity (denoted by the overbar), and the intensity spread within the template is taken into account by the lower part of the fraction in Eq. 2. Radiometric calibration of imagery is thus not needed. In its current form, all intensities are weighted equally, however, in the case of river ice velocity, we focus on pixels that have ice floes within. If ice-floe pixels can be identified, then a map or matrix ($\mathbf{W}$) can be used as a weighting function. In this way, the similarity function puts more emphasis on ice-floe pixels instead of open water. This can be written as a weighted NCC, that is

$$\Theta_{pq} = \frac{\sum_{k,l}\mathbf{W}_q(k,l)(\mathbf{I}_p(i+k,j+l) - \widetilde{\mathbf{I}}_p)(\mathbf{I}_q(k,l) - \widetilde{\mathbf{I}}_q)}{\sqrt{\sum_{k,l}\mathbf{W}_q(k,l)(\mathbf{I}_p(i+k,j+l) - \widetilde{\mathbf{I}}_p)^2 \sum_{k,l}\mathbf{W}_q(k,l)(\mathbf{I}_q(k,l) - \widetilde{\mathbf{I}}_q)^2}}. \tag{3}$$

Here a similar formulation is presented as in Eq. 2, though the intensity variations are weighted. These weights are normalized so their summation adds up to unity. The specific weights come from the entropy map ($\mathbf{W}_q = \prod p(\mathbf{H}_q)$), that was already used for the location selection of the central pixel. Another option would be to set intensity as the weighting map ($\mathbf{W}_q = \mathbf{I}$), but this will also put emphasis on homogeneously reflecting stagnant border ice. The weights stem only from one image ($\mathbf{W}_q$) in this formulation. Thus, we use entropy responses from the medium resolution Sentinel-2, while a template from the coarse resolution PROBA-V imagery functions as the search space ($\mathbf{I}_p$).

The highest value in the search space of the correlation score is selected. The distance between the seed location and this position is calculated and divided by the time separation to get the velocity.

Both Sentinel-2 and PROBA-V have multi-spectral instruments and in this case we use the red band. The blue band is not a favorable band for image matching, as in the PROBA-V processor a high compression ratio is implemented and in general this band has less high-resolution features (Dierckx et al., 2014). The red band of PROBA-V has a high signal-to-noise level and thus has most contrast between snow and water. This is less the case for the NIR channel (see also Table 1).

4.3. River ice velocity post-processing

As in any measurement, errors are present in the resulting product. These errors are a combination of random noise and gross outliers. It is quite typical for displacement estimates from optical remote sensing to be corrupted by a considerable amount of gross errors. Zonal statistics are typically implemented to improve such products (Lavergne et al., 2010), but due to the irregular sampling of our data, auxiliary information in the form of river outlines are used. The filtering is done through a comparison between individual flow estimates against the general flow direction (or heading). The general heading is extracted from the center line of the river (or thalweg) through mathematical morphology.

Our starting point is the river mask that is also used in the previous step (Allen and Pavelsky, 2018). The deltas and islands over this section

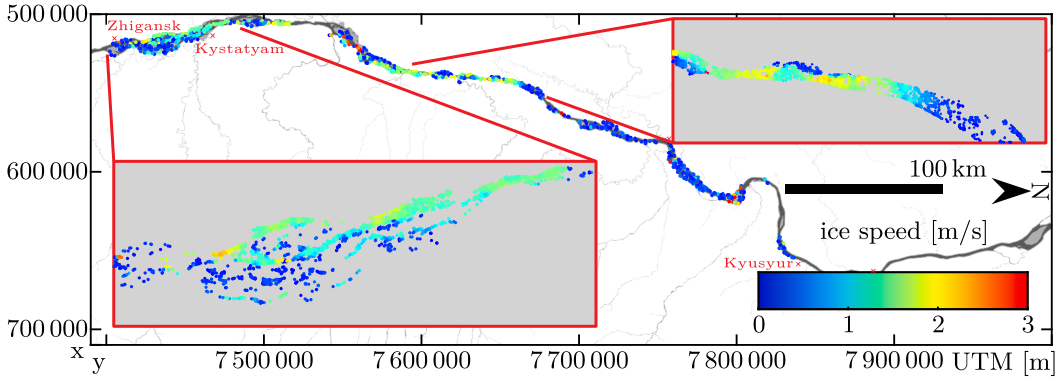

Fig. 6. River ice flow speed on the 25th of May 2016.

have somewhat changed, thus these are filled. Neighboring smaller rivers are then removed through an erosion operation. From this binary mask a skeleton is extracted through iterative erosion, creating a network with branches when the river widens. These small branches are removed by detecting endpoints, resulting in a center-line throughout the river that is used to fit a spline. The right-angled orientation of this spline is used to estimate the general flow direction of the study river, as is also shown in Fig. 5. This general flow direction is used to filter deflected velocity estimates, by comparing the relative angle which should not exceed 30°.

5. Results

Imagery from the 25th & 28th of May 2016 are used in this study. At that time the temporal acquisition spacing between PROBA-V and Sentinel-2 was 196.83 s (Fig. 2). The template width for the matching performed corresponds to six PROBA-V pixels, or ≈600 m, while the search space was limited to speeds up to 15 m/s. The PROBA-V image strip was interpolated to 10 m pixel size, in order to be at the same resolution as the Sentinel-2 image. Both images where transformed into the same Universal Transverse Mercator (UTM) projection. For Sentinel-2 several image tiles had to be combined, while for PROBA-V the full sunlit track is provided and only a subset was taken.

5.1. Co-registration of the satellite imagery

There can be substantial artificial movement between paired images. Absolute co-registration errors are caused by instrument noise from the positioning and orientation sensors in the satellite. For PROBA-V, the reported daily mean absolute location error over global landmarks for the red band data of the L2-product on the 25th of May 2016 is 73.25 m (N = 56,922, σ = 78.60), while on the 28th this is 90.59 m (N = 54,995, σ = 80.44) (Sterckx et al., 2016).

Compensation for co-registration offsets is done through displacement estimation over a relatively flat part along the river banks. A translation in the same order is found, for both the image pairs of the 25th (X: +20 m,Y: −160 m) as well as the pair of the 28th (X: +110 m,Y: −80 m). The co-registration offsets are assumed to be constants (simple translation), and can thus be subtracted from the displacement estimates over the river. Thus we are confident that additional motion present in the data stems from river ice movement.

5.2. River ice velocities on the 25th of May 2016

A total of 147,943 displacement estimates are calculated over the almost 700 km long river reach. After adjustment of the co-registration bias, a heading filter is applied over the raw displacement estimates, in order to exclude estimates deviating more than 30° from the main heading. An additional speed limit of 5 m/s is also imposed on the displacement estimates. These filters removed potential outliers, leaving 55% of the original estimates within the collection. The resulting displacements over this river reach are shown in Fig. 6 and its heading in Fig. 7.

On the 25th of May 2016, the southern part of our study region contained mobile ice. In contrast, the northern part of the river border ice has melted away and open leads are present, though the ice cover still seems to consist of intact stationary ice. Transverse cracks seem to be absent (though just north of Siktyakh, clouds obstruct the view), however this ice cover might be weak as small melt ponds do appear at the surface. One could expect transverse cracks to be present, as water levels are an important control on the creation of such instabilities. At this time such hinge cracks are not observed yet, indicating the ice cover is not very fragile.

The large intact ice cover in the northern part of the study reach is in

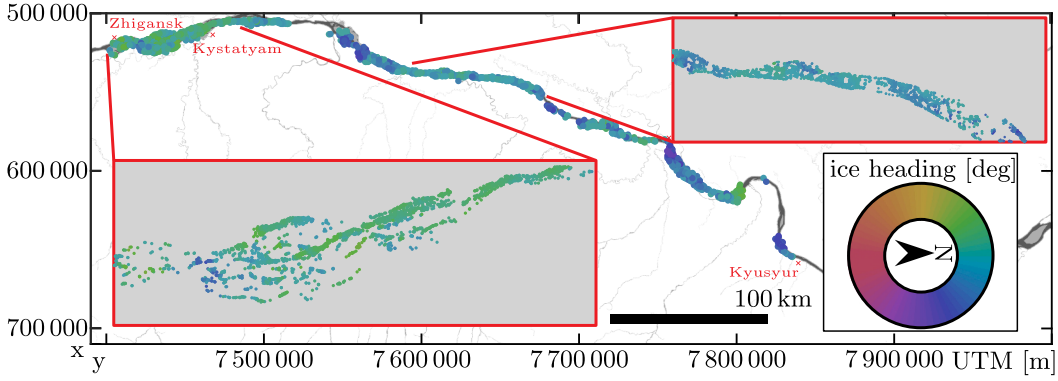

Fig. 7. River ice flow heading on the 25th of May 2016.

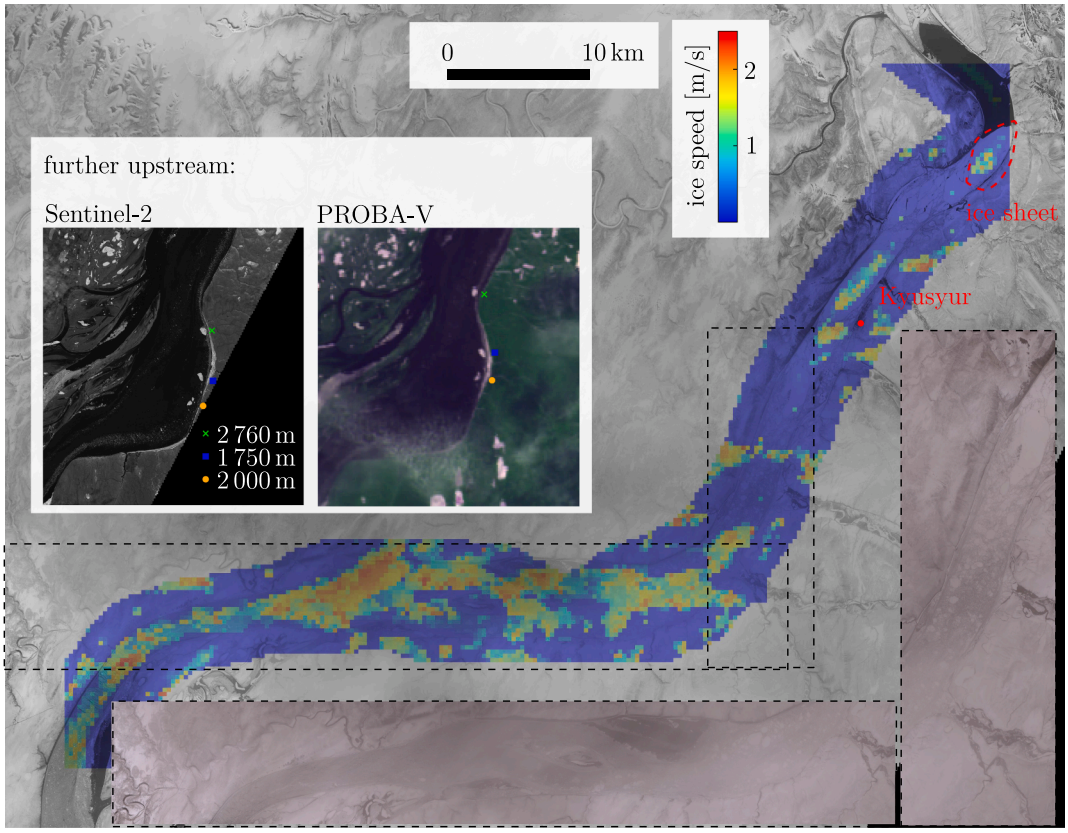

Fig. 8. River ice velocities on the 28th of May 2016, along a section where a ice jam is present. In the inset are two subsets shown hundreds of kilometers downstream, where ice clearing has occurred and ice floes move rapidly along. The location of both images are indicated in Fig. 5.

stark contrast to the broken-up southern region, where ice clearing has occurred and ice floes that are sporadically present rarely exceed 100 m in diameter and mostly ice debris is transported. The amount and size of ice floes gradually increase as one travels along-flow northwards, where ice floes and ice sheets eventually accumulate (upper right inset of Fig. 6). This congestion configuration looks very similar to the situation observed by Kääb et al. (2013) in 2011. Where a leading ice edge does seem to propagate upstream by juxtaposition, as a smooth transition of velocity is observable where ice pans come to a halt. Ice shoving (where ice floes are under-turning due to fast flow) occurs at velocities higher than 0.9 m/s, while under-ice flow can occur from 1.2 m/s onwards (US. Army Corps of Engineers, 2002). Given these velocities found in our data, one can expect these processes occur here as well. The river channel is relatively straight and of low slope and curvature, thus external forcing is relatively homogeneous. The further progression of this break-up might thus be driven by incoming water, causing vertical bending and producing a wedge to fracture the ice cover (Beltaos, 1997).

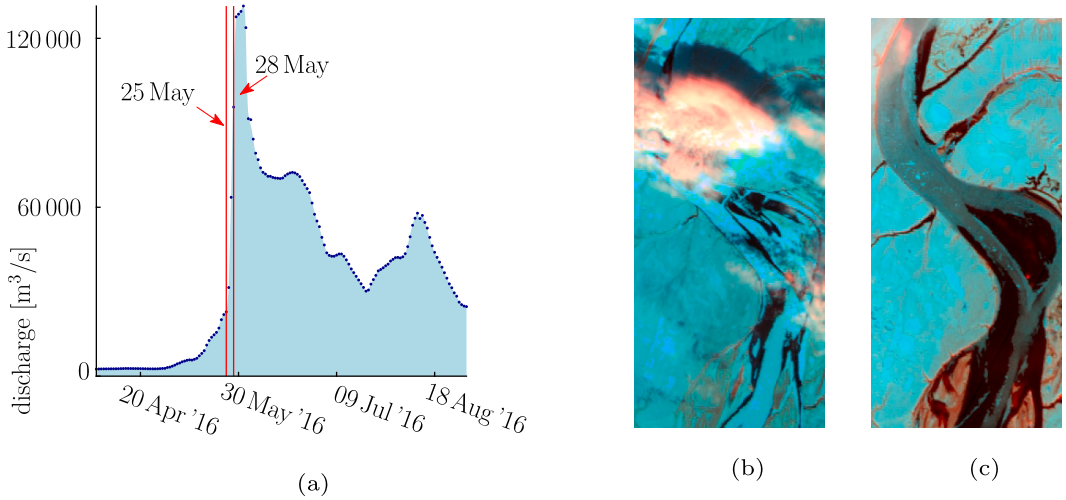

Fig. 9. (a) Daily discharge estimates near Kusur station, data from (Shiklomanov et al., 2018). (b, c) False color composite of PROBA-V at the location of the second ice jam. On the 25th of May 2016 (b) the water levels/extent is significantly lower, while on the 28th of May 2016 (c) more melt has occurred, but also water levels have risen.

5.3. River ice velocities on the 28th of May 2016

On the 28th of May 2016, an intact ice sheet is still present from the Lena delta in the north, all the way up to the village of Chekurovka. Here, ice sheets are stuck in the bends of the river, resulting in a small ice accumulation at the first bend, while a larger ice jam is formed upstream from Kyusyur. A large ice sheet is unable to maneuver through the turn, while more than 40 km of ice pans and debris accumulate behind this ice sheet (Fig. 8). Unfortunately, high clouds obstruct a clear view on the ice congestion, so results from the entropy filter are low in these parts. Therefore, naive image matching on a regular grid is applied here (Eq. 2), and no post-processing is applied. Results from the first two bands of PROBA-V are used, as the others are more sensitive to clouds and contrast is low. Still, some velocities can be estimated from these cloudy imagery, though outliers occur on the homogeneous reflecting large ice sheet or the dark water in-between the jams.

Further downstream, just before the village of Zhigansk, the river transported or melted most of its ice cover, and small rubble occupies a small strip of the river. Here, the velocities of the river ice are substantial, visual inspection on the sparsely present ice floes along the shoreline show speeds in the order of 10 m/s (see also the inset of Fig. 8). Such flow velocities are twice as fast as an ice break-up event, hence the water pressure of the ice jam will build up even more. Because of its fast flow with strong velocity gradients and mixture, in combination with coarse resolution acquisitions from PROBA-V, the image matching over these regions gives very few good displacement estimates.

6. Discussion

Daily discharge estimates for Lena River near the village of Kuysuyr are shown in Fig. 9a. The discharge has gradually increased until the 25th of May 2016, afterwards it rises substantially. On the 28th of May 2016 the peak discharge is almost reached, which does coincide with the ice clearance seen in the satellite imagery. This substantial increase of discharge is also evident by the flooding along the banks of the river (Fig. 9c). In this section the ice floes start to slow down into stagnant ice. The water level in the adjacent tributary rivers have risen, as their extent has broadened.

6.1. Factors influencing the performance of velocity extraction

What is also evident from the inset of Fig. 8, is the limitations posed by the coarse resolution of PROBA-V imagery. When sufficient velocity and time separation is present, the ice debris mixes considerably and the inhomogenous movement makes the ice rubble indistinguishable from one another. In those cases, it seems the pattern matching generates high scores along the edge of the ice debris. It locks on this edge and is also influenced by within-pixel texture. This happens extensively in data from 2017, see Fig. 4. Higher resolution data are in these cases more sufficient, such as is for example done with the commercial 3-meter resolution cubesat constellation of Planet (Kääb et al., 2019). Images during freeze-up could produce better results since there are more frazil pans than ice debris (Kääb et al., 2019). However, river ice break-ups in winter are more rare (Prowse et al., 2007).

Though of coarse resolution, the seemingly large amount of correct velocities of the early break-up on the 25th of May 2016 from PROBA-V and Sentinel-2 data, show the time span can be in the order of some minutes. A shorter interval (in the order of 30 s) might give consistently good results for the whole break-up cycle. Though this would lower the theoretical precision of the velocity measurements, as this is now in the order of the pixel resolution (10 m). This currently results in a theoretical precision of $\pm\frac{1}{20}$ m/s, but would increase to $\frac{1}{3}$ m/s.

The directional filter seems to be a robust, efficient and simple post-processing procedure to implement. Filtering by keeping only displacements with high correlation scores is not done here, because there

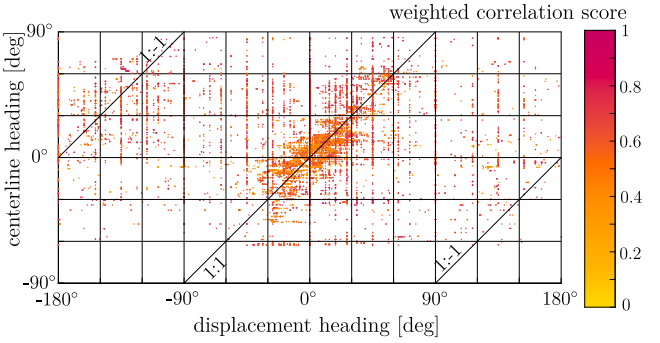

Fig. 10. Scatter plot between measured heading and direction of the thalweg, on estimates from the 25th of May 2016.

is a weighting within the similarity estimation. Thus the score is not an absolute measure, which can also be observed in Fig. 10. The illustration shows the individual displacement headings in relation to the thalweg direction. Points in the figure are color-coded based upon their weighted correlation score (Eq. 3), but no clear relation seems to be present. Correlation score is thus not a stable quality indicator, while this is the case for the thalweg direction. The main spread seems to fall on the 1:1 line or at least in between 30° of this line. Apart from a clear correlation, a slight preference for the reverse direction of flow can be observed. These rough velocities are going in straight opposite direction of the general flow direction. Such estimates are the result of sensitivities to the water edge and homogeneous ice debris as described above.

The selection for template locations based upon finding ice floes through entropy filters, lowers the computational cost and can thus be done on the fly. More detailed velocity fields can be estimated, but the computational time will be some orders slower due to naive matching on a predefined grid. However, the coarse resolution of PROBA-V and the velocity gradients at the river do result in a lower amount of matches and outliers are still present, especially when the river clearing of ice is far advanced (as is the case on th 28th of May). Hence, expert knowledge is needed to finally interpret the displacement estimates. But such expert interpretation seems reasonable within a framework of risk assessments, where potential jam locations need to be identified. In this respect, our product can provide additional insights, and can be used on the same day to task a detailed very-high resolution near-simultaneous image acquisition or optical video from an afternoon pass. Such afternoon systems, like Skysat, are already in space (d'Angelo et al., 2016). This proposed, data-driven procedure is not yet adopted within the river-ice community (Rokaya et al., 2018), but we hope this work will demonstrate its potential.

6.2. The potential for other optical remote sensing combinations

In this study we show the potential use of imagery from different platforms, at different spatial resolution within a sun synchronous orbit. Since many optical sensors are within a similar sun-synchronous orbit with akin inclination and overpass time, the concept of mapping river ice velocities can be extended to other satellite combinations.

In order to be of wide use two issues need to be taken care of: i; rapid and open access of the data and ii; coordination between satellite operators. For example, the Chinese government has recently opened their data archive of GaoFen-1, which is very encouraging. However, this also demonstrates the necessity of the second point, being coordination. GaoFen-1 WFV is a 16 meter resolution multi-spectral imager, with a wide swath of roughly 800 km and imaging capacity of 20,000 km/day alongtrack, while orbit maneuvers are done once a month (Chunling and Zhaoguang, 2015). Hence, this could be an ideal companion satellite for Sentinel-2 to monitor river ice. However, more coordination might be needed, as already shown in this study as well, ice pans and ice floes

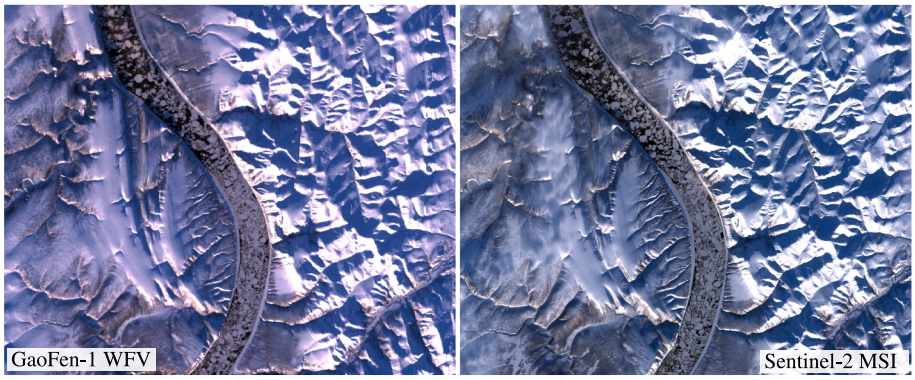

Fig. 11. Example of frazil floes and skim ice traveling through the bend close to the city of Chekurovka, Lena River, on the 21st of October 2017.

have complicated flows due to their interaction. For example to illustrate this set-up, Fig. 11 shows an overpass of Sentinel-2 and GaoFen-1 on the 21st of October 2017 just north of the Lena reach under study here. In this case the time difference is roughly 240 s. Ice floes can be identified but the time separation causes too much displacement for pattern matching to be used. Some floes rotate, different floes move at different velocities, and thus a shorter interval would make such a combination possible. Similar problems were present for the data from PROBA-V and Sentinel-2 in spring 2017, where low success rates were caused by a too long time difference of 567.4 s (the imagery in Fig. 4 are from this combination).

7. Conclusions

In this study we automatically extract river ice velocities for the Lena River over several hundreds of kilometers from medium and coarse resolution optical remote sensing data. For clear imagery or imagery with thin clouds, our image matching implementation is able to extract velocities over a large cross profile of the river. Due to the large amount of ice rubble, a two dimensional flow field behind two ice jams on the 25th and 28th of May 2016 could be extracted. However, with the coarse resolution imagery of PROBA-V it was complicated to track sparse ice debris and other small drifting features. This occurs when the break-up is at a later stage and ice clearance only transports small-diameter ice debris on the surface. Still, the coarse resolution imagery is able to generate velocity estimates at congestion zones where ice jams develop. These regions are of most interest and our study shows a next step towards consistent documentation of river ice break-ups, which is essential to understand the complexities of such dynamics (Hicks, 2009).

This study demonstrates the great value of multi-sensor integration, which has in recent years become feasible because of the large amount of satellites dedicated to large scale monitoring. However, this potential for a service might also be leveraged from another branch of satellite systems: small-satellites to nano-satellites. Just a couple of years ago, these smaller satellites were not yet in space (Guerra et al., 2016), but currently the cost for access to space is lowering. These smaller satellite missions can fly in pair with dedicated missions, and this seems already the case for the Landmapper-BC system, which is a growing constellation of medium resolution satellites (22 meter), focused on a similar crossing time as the Landsat and Sentinel-2 systems.

Given that coarse resolution satellites have been shown to be able to extract velocity information on a vast ice shelf (Haug et al., 2010) and now on Arctic rivers, we see a great geometrical potential for coarse resolution optical spaceborne systems. While PROBA-V has a 100 meter nadir resolution, the Sentinel-3 mission has 300 meter, but is sustainable in its orbital overpassing. It might be a candidate satellite combination for this application, as it can be combined with ESA's soon to be launched Earth Explorer 8 which will be in the same orbit, but with 15 s in advance of Sentinel-3 (Drusch et al., 2016). As both missions have open data policy, it will likely be possible to generate an added-value service out of this combination. We hope this example shows the potential of a holistic view on Earth observation and not only considering the different instruments on Sentinel-3 for river discharge (Tarpanelli et al., 2019), but also exploit instruments on other satellites like FLEX.

For PROBA-V the mission has finished its operational phase and has moved into its experimental phase, where it will have a companion satellite flying along. At the time of writing not much information is available, but it is envisioned to fly along a cubesat with first an optical and later a thermal payload. Our study shows the feasibility to detect river-ice movement with such coarse resolution sensors. In order to get the same product, we think the mission objective can be simple, thus an off-the-shelf camera will be sufficient, either visible (Holmes et al., 2018) or hyperspectral (Esposito et al., 2018). Our study shows, such a configuration of near-simultaneous satellites is able to generate a river ice monitoring product in a semi-automatic manner, increasing the product portfolio of such missions.

CRediT authorship contribution statement

Bas Altena: Conceptualization, Methodology, Investigation, Writing - original draft. **Andreas Kääb:** Writing - review & editing.

Declaration of Competing Interest

The authors declare that they have no known competing financial interests or personal relationships that could have appeared to influence the work reported in this paper.

Acknowledgement

We like to thank two anonymous reviewers for their input, which helped to improve the manuscript, Freysteinn Sigmundsson and Jonathan Li for handling the review process as editor. This research and development has been conducted through support from the European Union FP7 ERC project ICEMASS (320816), a ESA Living Planet Fellowship and a Netherlands space office (NSO) project (ALWGO.2018.044) to B.A., Glaciers-CCI, CCI+ and EE10 HARMONY projects (4000125560/18/I-NS, 4000109873/14/I-NB, 4000127593/19/I/NB, 4000127656/19/NL/FF/gp).

Appendix A

Information about the imagery data used in this study is given here. The first image of Sentinel-2 was taken on the 25th of May 2016, while in satellite orbit row 104, and tile numbers:

T51WWQ, T51WWR, T51WWS, T51WWT,
T51WWU, T51WWV, T51WXR, T51WXS,
T51WXT, T51WXU, T51WXV & T52WDB cover Lena river.

For the 28th of May acquisition, the satellite was in orbit row 004, and tile numbers:

T51WWR, T51WWS, T51WWT, T51WWU,
T51WXT, T51WXU & T51WXV

are partly or entirely cloud free, the smaller number of tiles is due to cloud cover at this date. The image identifiers for the PROBA-V imagery used are:

PROBAV_L2A_20160525_034349_2_100M_V101
PROBAV_L2A_20160528_041754_2_100M_V101

After signing in, these can be downloaded from www.vito-eodata.be/PDF/portal/Application.html

References

Allen, G.H., Pavelsky, T.M., 2018. Global extent of rivers and streams. Science 361 (6402), 585–588. https://doi.org/10.1126/science.aat0636.

Allen, G.H., David, C.H., Andreadis, K.M., Hossain, F., Famiglietti, J.S., 2018. Global estimates of river flow wave travel times and implications for low-latency satellite data. Geophys. Res. Lett. 45, 7551–7560. https://doi.org/10.1029/2018GL077914.

Beltaos, S., 1997. Onset of river ice breakup. Cold Reg. Sci. Technol. 25 (3), 183–196. https://doi.org/10.1016/S0165-232X(96)00011-0.

Beltaos, S., Burrell, B.C., 2005. Determining ice-jam-surge characteristics from measured wave forms. Can. J. Civ. Eng. 32 (4), 687–698. https://doi.org/10.1139/l05-019.

Beltaos, S., Kääb, A., 2014. Estimating river discharge during ice breakup from near-simultaneous satellite imagery. Cold Reg. Sci. Technol. 98, 35–46. https://doi.org/10.1016/j.coldregions.2013.10.010.

Brown, L.G., 1992. A survey of image registration techniques. ACM Comput. Surv. (CSUR) 24 (4), 325–376. https://doi.org/10.1145/146370.146374.

Chaouch, N., Temimi, M., Romanov, P., Cabrera, R., McKillop, G., Khanbilvardi, R., 2014. An automated algorithm for river ice monitoring over the Susquehanna river using the MODIS data. Hydrol. Process. 28 (1), 62–73. https://doi.org/10.1002/hyp.9548.

Choe, B-H, Samsonov, S.V., Jung, J., 2020. Landfast ice growth and displacement in the Mackenzie Delta observed by 3D time-series SAR speckle offset tracking. Cryosphere Discuss. 1–19. https://doi.org/10.5194/tc-2020-116.

Chunling, L., Zhaoguang, B., 2015. Characteristics and typical applications of GF-1 satellite. In: International Geoscience and Remote Sensing Symposium (IGARSS). IEEE, pp. 1246–1249. https://doi.org/10.1109/IGARSS.2015.7325999.

Cooley, S.W., Pavelsky, T.M., 2016. Spatial and temporal patterns in Arctic river ice breakup revealed by automated ice detection from MODIS imagery. Remote Sens. Environ. 175, 310–322. https://doi.org/10.1016/j.rse.2016.01.004.

d'Angelo, P., Máttyus, G., Reinartz, P., 2016. Skybox image and video product evaluation. Int. J. Image Data Fusion 7 (1), 3–18. https://doi.org/10.1080/19479832.2015.1109565.

Dierckx, W., Sterckx, S., Benhadj, I., Livens, S., Duhoux, G., Van Achteren, T., Francois, M., Mellab, K., Saint, G., 2014. PROBA-V mission for global vegetation monitoring: standard products and image quality. Int. J. Remote Sens. 35 (7), 2589–2614. https://doi.org/10.1080/01431161.2014.883097.

Donlon, C., Berruti, B., Buongiorno, A., Ferreira, M.-H., Féménias, P., Frerick, J., Goryl, P., Klein, U., Laur, H., Mavrocordatos, C., Nieke, J., Rebhan, H., Seitz, B., Stroede, J., Sciarra, R., 2012. The global monitoring for environment and security (GMES) sentinel-3 mission. Remote Sens. Environ. 120, 37–57. https://doi.org/10.1016/j.rse.2011.07.024.

Drusch, M., Del Bello, U., Carlier, S., Colin, O., Fernandez, V., Gascon, F., Hoersch, B., Isola, C., Laberinti, P., Martimort, P., Meygret, A., Spoto, F., Sy, O., Marchese, F., Bargellini, P., 2012. Sentinel-2: ESA's optical high-resolution mission for GMES operational services. Remote Sens. Environ. 120, 25–36. https://doi.org/10.1016/j.rse.2011.11.026.

Drusch, M., Moreno, J., Del Bello, U., Franco, R., Goulas, Y., Huth, A., Kraft, S., Middleton, E.M., Miglietta, F., Mohammed, G., Nedbal, L., Rascher, U., Shüttemeyer, D., Verhoef, W., 2016. The fluorescence explorer mission concept - ESA's Earth explorer 8. IEEE Trans. Geosci. Remote Sens. 55 (3), 1273–1284. https://doi.org/10.1109/TGRS.2016.2621820.

Dugan, J.P., Anderson, S.P., Piotrowski, C.C., Zuckerman, S.B., 2013. Airborne infrared remote sensing of riverine currents. IEEE Trans. Geosci. Remote Sens. 52 (7), 3895–3907. https://doi.org/10.1109/TGRS.2013.2277815.

Esposito, M., Conticello, S., Vercruyssen, N., van Dijk, C., Foglia Manzillo, P., Koeleman, C., Delauré, B., Benhadj, I., Blommaert, J., Livens, S., Jochemsen, A., Soukup, M., Menenti, M., Gorte, B., Housseini, A., 2018. Demonstration in space of a smart hyperspectral imager for nanosatellites. In: 32nd Annual AIAA/USU Conference on Small Satellites, number SSC18-I-07, pp. 1–7. https://digitalcommons.usu.edu/smallsat/2018/all2018/257/.

Fedorova, I., Chetverova, A., Bolshiyanov, Dmitry, Makarov, A., Boike, Julia, Heim, Birgit, Morgenstern, Anne, Overduin, Paul P., Wegner, Carolyn, Kashina, V., et al., 2015. Lena delta hydrology and geochemistry: long-term hydrological data and recent field observations. Biogeosciences 12 (2), 345–363. https://doi.org/10.5194/bg-12-345-2015.

Francois, M., Santandrea, S., Mellab, K., Vrancken, D., Versluys, J., 2014. The PROBA-V mission: The space segment. Int. J. Remote Sens. 35 (7), 2548–2564. https://doi.org/10.1080/01431161.2014.883098.

Gascon, F., Bouzinac, C., Thépaut, O., Jung, M., Francesconi, B., Louis, J., Lonjou, V., Lafrance, B., Massera, S., Gaudel-Vacaresse, A., Languille, F., Alhammoud, B., Viallefont, F., Pflug, B., Bieniarz, J., Clerc, S., Pessiot, L., Trémas, T., Cadau, E., De Bonis, R., Isola, C., Martimort, P., Fernandez, V., 2017. Copernicus Sentinel-2A calibration and products validation status. Remote Sens. 9 (6), 584. https://doi.org/10.3390/rs9060584.

Gautier, E., Dépret, T., Costard, F., Virmoux, C., Fedorov, A., Grancher, D., Konstantinov, P., Brunstein, D., 2018. Going with the flow: Hydrologic response of middle Lena River (Siberia) to the climate variability and change. J. Hydrol. 557, 475–488. https://doi.org/10.1016/j.jhydrol.2017.12.034.

Gleason, C.J., Smith, L.C., 2013. Toward global mapping of river discharge using satellite images and at-many-stations hydraulic geometry. Proc. Natl. Acad. Sci. https://doi.org/10.1073/pnas.1317606111.

Gonzalez, R.C., Woods, R.E., 2002. Digital image processing. Prentice Hall, New Jersey.

Guerra, André G.C., Francisco, Frederico, Villate, Jaime, Agelet, Fernando Aguado, Bertolami, Orfeu, Rajan, Kanna, 2016. On small satellites for oceanography: A survey. Acta Astronaut. 127, 404–423. https://doi.org/10.1016/j.actaastro.2016.06.007.

Haug, T., Kääb, A., Skvarca, P., 2010. Monitoring ice shelf velocities from repeat MODIS and Landsat data–a method study on the Larsen C ice shelf, Antarctic Peninsula, and 10 other ice shelves around Antarctica. Cryosphere 4 (2), 161–178. https://doi.org/10.5194/tc-4-161-2010.

Hawotte, F., Radoux, J., Chomé, G., Defourny, P., 2016. Assessment of automated snow cover detection at high solar zenith angles with PROBA-V. Remote Sens. 8 (9), 699. https://doi.org/10.3390/rs8090699.

Hicks, F., 2009. An overview of river ice problems: Cripe07 guest editorial. Cold Reg. Sci. Technol. 55 (2), 175–185. https://doi.org/10.1016/j.coldregions.2008.09.006.

Holmes, A., Morrison, J.M., Feldman, G., Patt, F., Lee, S., 2018. Hawkeye ocean color instrument: performance summary. In: CubeSats and NanoSats for Remote Sensing II, vol. 10769. International Society for Optics and Photonics, p. 107690C. https://doi.org/10.1117/12.2320654.

Huang, C., Chen, Y., Zhang, S., Wu, J., 2018. Detecting, extracting, and monitoring surface water from space using optical sensors: A review. Rev. Geophys. 56, 333–360. https://doi.org/10.1029/2018RG000598.

Hudson, C.E., Thompson, J.R., 2019. Hydrological modelling of climate change impacts on river flows in Siberia's Lena River basin and implications for the Atlantic Meridional Overturning Circulation. Hydrol. Res. 50 (6), 1577–1595. https://doi.org/10.2166/nh.2019.151.

Kääb, A., Leprince, S., 2014. Motion detection using near-simultaneous satellite acquisitions. Remote Sens. Environ. 154, 164–179. https://doi.org/10.1016/j.rse.2014.08.015.

Kääb, A., Prowse, T., 2011. Cold-regions river flow observed from space. Geophys. Res. Lett. 38 (8) https://doi.org/10.1029/2011GL047022.

Kääb, A., Lamare, M., Abrams, M., 2013. River ice flux and water velocities along a 600 km-long reach of Lena river, Siberia, from satellite stereo. Hydrol. Earth Syst. Sci. 17, 4671–4683. https://doi.org/10.5194/hess-17-4671-2013.

Kääb, A., Winsvold, S.H., Altena, B., Nuth, C., Nagler, T., Wuite, J., 2016. Glacier remote sensing using Sentinel-2. Part I: Radiometric and geometric performance, and application to ice velocity. Remote Sens. 8 (7), 2072–4292. https://doi.org/10.3390/rs8070598.

Kääb, A., Altena, B., Mascaro, J., 2019. River ice and water velocities using the Planet optical cubesat constellation. Hydrol. Earth Syst. Sci. 23, 4233–4247. https://doi.org/10.5194/hess-23-4233-2019.

Kowalczyk Hutchison, T., Hicks, F.E., 2007. Observations of ice jam release waves on the Athabasca River near Fort McMurray, Alberta. Can. J. Civ. Eng. 34 (4), 473–484. https://doi.org/10.1139/l06-144.

Kræmer, T., Johnsen, H., Brekke, C., Engen, G., 2017. Comparing SAR-based short time-lag cross correlation and Doppler-derived sea ice drift velocities. IEEE Trans. Geosci. Remote Sens. 56 (4), 1898–1908. https://doi.org/10.1109/TGRS.2017.2769222.

Lavergne, T., Eastwood, S., Teffah, Z., Schyberg, H., Breivik, L.-A., 2010. Sea ice motion from low-resolution satellite sensors: An alternative method and its validation in the Arctic. J. Geophys. Res. Oceans 115 (C10). https://doi.org/10.1029/2009JC005958.

Lewis, Q.W., Rhoads, B.L., 2018. LSPIV measurements of two-dimensional flow structure in streams using small unmanned aerial systems: 2. Hydrodynamic mapping at river confluences. Water Resour. Res. 54 (10), 7981–7999. https://doi.org/10.1029/2018WR022551.

Lindenschmidt, K.-E., Das, A., 2015. A geospatial model to determine patterns of ice cover breakup along the Slave river. Can. J. Civ. Eng. 42 (9), 675–685. https://doi.org/10.1139/cjce-2014-0377.

Prowse, T.D., Bonsal, B.R., Duguay, C.R., Lacroix, M.P., 2007. River-ice break-up/freeze-up: a review of climatic drivers, historical trends and future predictions. Ann. Glaciol. 46, 443–451. https://doi.org/10.3189/172756407782871431.

Rokaya, P., Budhathoki, S., Lindenschmidt, K.-E., 2018. Ice-jam flood research: a scoping review. Nat. Hazards 94 (3), 1439–1457. https://doi.org/10.1007/s11069-018-3455-0.

Shiklomanov, A.I., Holmes, R.M., McClelland, J.W., Tank, S.E., Spencer, R.G.M., 2018. Arctic great rivers observatory. discharge dataset. URL https://www.arcticrivers.org/data.

Smith, L.C., Pavelsky, T.M., 2008. Estimation of river discharge, propagation speed, and hydraulic geometry from space: Lena River, Siberia. Water Resour. Res. 44 (3) https://doi.org/10.1029/2007WR006133.

Sterckx, S., Adriaensen, S., Sima, A., 2016. PROBA-V quarterly image quality report. Technical Report 10, VITO - vlaams instituut voor technologisch onderzoek. http://proba-v.vgt.vito.be/sites/proba-v.vgt.vito.be/files/documents/probav_d9_qir-010_2016-q2_v1.0_0.pdf.

Tarpanelli, A., Camici, S., Nielsen, K., Brocca, L., Moramarco, T., Benveniste, J., 2019. Potentials and limitations of Sentinel-3 for river discharge assessment. Adv. Space Res. https://doi.org/10.1016/j.asr.2019.08.005.

US. Army Corps of Engineers, 2002. Ice engineering manual. CECW-EH 1110-2-1612, Department of the Army.
Vincent, F., Raucoules, D., Degroeve, T., Edwards, G., Abolfazl Mostafavi, M., 2004. Detection of river/sea ice deformation using satellite interferometry: limits and potential. Int. J. Remote Sens. 25 (18), 3555–3571. https://doi.org/10.1080/01431160410001688303.
Ye, H., Ladochy, S., Yang, D., Zhang, T., Zhang, X., Ellison, M., 2004. The impact of climatic conditions on seasonal river discharges in Siberia. J. Hydrometeorol. 5 (2), 286–295. https://doi.org/10.1175/1525-7541(2004)005<0286:TIOCCO>2.0.CO;2.
Zhang, F., Mosaffa, M., Chu, T., Lindenschmidt, K.-E., 2017. Using remote sensing data to parameterize ice jam modeling for a northern inland delta. Water 9 (5), 306. https://doi.org/10.3390/w9050306.